EAI Endorsed Transactions
on Transportation Systems and Ocean Engineering
Review Article EAI.EU

High-Speed Train Braking Control: Applications and CTD4–Digital Twin Perspectives for Operational Safety

Duc-Quy Nguyen[1,2*], Ngo Manh Dung[3], Ngoc-Thuan Nguyen[1]

[1]AIT Research Group, University of Transport Ho Chi Minh City, Ho Chi Minh City, Vietnam
[2]Faculty of Engineering, Dong Nai Technology University, Dong Nai City, Vietnam
[3]Ho Chi Minh City University of Technology, VNU-HCM, Ho Chi Minh City, Vietnam

Abstract

The braking system directly determines the stopping capability, adhesion utilization, and operational safety of high-speed trains. However, braking performance is simultaneously affected by electric–pneumatic braking-force distribution, actuator delay, wheelset dynamics, and wheel-rail adhesion that varies with speed and contact conditions. This paper first systematizes the braking structure at three levels: vehicle, carriage, and wheel, while summarizing the longitudinal dynamics, slip-ratio formulation, and wheel-rail adhesion characteristics to define the feasible braking domain. On this basis, artificial-intelligence approaches are reviewed according to three levels of development: machine learning (ML) for estimation, deep learning (DL) for representation learning, and deep reinforcement learning (DRL) for sequential braking decision-making. The analysis shows that ML and DL improve the estimation of adhesion, stopping response, and wheel-slip conditions, whereas DRL extends toward direct traction/braking command generation; however, the physical feasibility of the resulting actions is not guaranteed when adhesion and actuator states vary outside the training domain. To address this gap, the paper proposes a conceptual CTD4–Digital Twin framework in which the twin updates physical states and parameters, CTD4 learns the return distribution under uncertainty, and a safety projection constrains the action before it is transmitted to the braking system.

Received on 14 October 2026; accepted on 09 November 2026; published on 12 November 2026

Keywords: high-speed train, braking control, wheel–rail adhesion, wheel-slide protection, CTD4, Digital Twin

Copyright © 2026 Duc-Quy Nguyen *et al.*, licensed to EAI. This is an open access article distributed under the terms of the CC BY-NC-SA 4.0, which permits copying, redistributing, remixing, transformation, and building upon the material in any medium so long as the original work is properly cited..

doi:10.4108/tsoe.15540

1. Introduction

High-speed train (HST) braking requires stopping accuracy, stable wheel–rail adhesion, and appropriate force distribution [1], [2], [3]. Performance depends on axle-load transfer, force allocation, and actuator dynamics [4], [5], [6], together with slip, adhesion variation, and state-dependent parameters [7], [8], [9]. Experiments confirm that adhesion varies with creepage and surface conditions [10].

Several control methods have been studied for HSTs to improve speed tracking and handle constraints [11]. PID controllers are still used for speed tracking [12], while fuzzy model predictive control (MPC), adaptive fuzzy sliding-mode control, and terminal sliding-mode control have been applied to deal with nonlinearities and uncertainties [13], [14], [15]. Other methods include model-free adaptive robust control, predictive sliding-mode control, and MPC for braking-force distribution [16], [17], [18]. Studies in other fields have also considered constrained MPC, fault-tolerant control, and optimization under actuator limitations [19], [20], [21]. Model-based control combined with deep learning, neural networks, and learning-based control has also been investigated [22], [23], [24].

Machine learning (ML) and deep learning (DL) support stopping-point prediction [25], wheel-slip detection [26], and adhesion estimation [27]. Deep reinforcement learning (DRL) instead learns control actions through

*Corresponding author. Email: nguyenducquy@dntu.edu.vn

environmental interaction; railway applications are reviewed in [28]. Examples include trajectory optimization [29], continuous control using TD3 [30], and safe RL under operational constraints [31]. However, commands may become inappropriate when adhesion or actuator conditions change.

Digital Twin (DT) applications in railways are reviewed in [32], [33]. In braking systems, DT can update estimates of wheel slip, brake pressure, adhesion, and actuator states. Ershenko et al. examined its use in braking-system verification and decision-making [34]. ML/DL methods mainly support estimation and prediction, while DRL generates control decisions and DT updates the physical model.

Table 1 brings together representative model-based, ML/DL, DRL, and DT studies relevant to high-speed train braking. The studies were selected according to their methodological contributions, reported results, and limitations. The table compares their roles and quantitative performance, with attention to adaptation under changing adhesion conditions and the requirements of braking efficiency and safety.

Combining online model updates with learning-based control remains a challenge when braking commands must satisfy physical limits. This paper reviews the braking-system structure and dynamics alongside model-based, ML/DL, and DRL methods. It then proposes a conceptual CTD4–Digital Twin framework: DT updates physical states and parameters, CTD4 generates commands through distributional policy learning, and a safety projection restricts the commands to the estimated feasible action set.

2. Structure and Dynamics of the Braking System

The braking system of a HST can be considered at three decision levels. At the vehicle level, the braking trajectory is determined based on stopping distance, speed limits, gradient, and timetable. At the carriage level, the total braking force is distributed among the carriages and between electric braking (EB) and air braking (AB).

At the vehicle level, the time–distance relationship is expressed as

$$\frac{dt}{dx} = \frac{1}{v}, \tag{1}$$

and the longitudinal dynamics are described by

$$mv\frac{dv}{dx} = -u(x) - F^r(x) - F^g(x). \tag{2}$$

The Davis resistance is given by

$$F^r(x) = m\left(c_0 + c_1 v + c_2 v^2\right), \tag{3}$$

while the gradient resistance is determined by

$$F^g(x) = mg\sin\alpha(x) \tag{4}$$

where t denotes time; x is the longitudinal position along the track; v is the longitudinal speed of the train; m is the train mass; u is the nonnegative magnitude of the total braking force acting opposite to forward motion; $F^r(x)$ and $F^g(x)$ denote the Davis resistance and gradient resistance, respectively; c_0, c_1, and c_2 are the Davis coefficients; g is the gravitational acceleration; and α is the track gradient angle. Train-operation and braking-control models use these longitudinal dynamic relationships to link the braking command with the speed–position evolution. However, the parameters of the train motion model need to be calibrated according to the specific train and operational data; the calibration of train motion models has been reviewed separately in the literature [39].

The positive longitudinal direction follows the train's forward motion. Thus, braking and Davis resistance enter Eq. (2) with negative signs. The gradient angle $\alpha(x)$ is positive uphill and negative downhill, so $-F^g(x)$ opposes motion uphill and assists it downhill. The position-domain equations apply for $v > 0$.

The total braking force consists of EB and AB.

$$u(x) = u^{\text{elec}}(x) + u^{\text{air}}(x), \tag{5}$$

subject to the following basic constraints

$$0 \le u^{\text{elec}} \le \sigma^{\text{elec}}(v), \qquad 0 \le u^{\text{air}} \le \sigma^{\text{air}} \tag{6}$$

where u^{elec} and u^{air} denote the electric and pneumatic braking forces, respectively; $\sigma^{\text{elec}}(v)$ is the speed-dependent electric-braking-force limit; and σ^{air} is the pneumatic-braking-force limit. During deceleration, the relative contributions of EB and AB vary across different operating stages. Figure 1 illustrates the three-stage coordinated braking strategy adopted in this study, consisting of regenerative braking, blended braking, and pneumatic braking.

Studies on braking-force distribution have shown that axle-load transfer and the braking-force limits of individual actuators should be explicitly considered in EB–AB coordination [5], [18]. For pneumatic braking, pressure propagation and air-brake dynamics may cause nonuniform braking responses along the train; freight-train air-brake models provide a modeling basis for this phenomenon [40]. In addition, emergency-braking modeling for HSTs has shown that some braking-model parameters may vary over time and therefore require online identification [9].

At the wheel level, the rotational dynamics of the wheelset are expressed as [7], [8]

$$I_w\dot{\omega}_i = T_{a,i} - T_{b,i}, \tag{7}$$

while the longitudinal dynamics of the carriage are given by

$$m_v\dot{v} = -\sum_{i=1}^{n} F_{a,i} - F_{\text{res}}. \tag{8}$$

Table 1. Representative approaches for railway braking-related control and their quantitative performance

Group	Representative studies	Main role	Quantitative performance	Main limitation
Model-based control	Wang and Tang [13]; Guo et al. [14]; Zhou et al. [17]; Wang et al. [18]	Tracking, robustness, and braking-force allocation	Tracking error, robustness, and constraint satisfaction; no unified benchmark	Depends on model accuracy and predefined constraints
ML/DL	Chen et al. [25]; Namoano et al. [26]; Zirek and Uysal [27]; Yang et al. [35]	Stopping prediction, wheel-slip detection, and adhesion estimation	Stopping error: ↓38.6–49.2% [25] (simulation using operational data); adhesion estimation: $R^2 = 0.922$ [27] (measured data)	Strongly dependent on training-data coverage
DRL	Ning et al. [29]; Zhou et al. [30]; Lin et al. [31]; Lu and Liu [36]	Trajectory optimization and continuous traction/braking decisions	Energy consumption: ↓15.75%; convergence speed: ↑37% [36] (simulation)	Reward optimization alone does not guarantee physical feasibility
DT / uncertainty-aware control	Jin et al. [9]; Ershenko et al. [34]; Peng et al. [37]; Valencia et al. [38]	State/model updating, health estimation, and uncertainty representation	Mainly validation and estimation metrics; no unified braking metric	Closed-loop integration with hard braking constraints remains limited

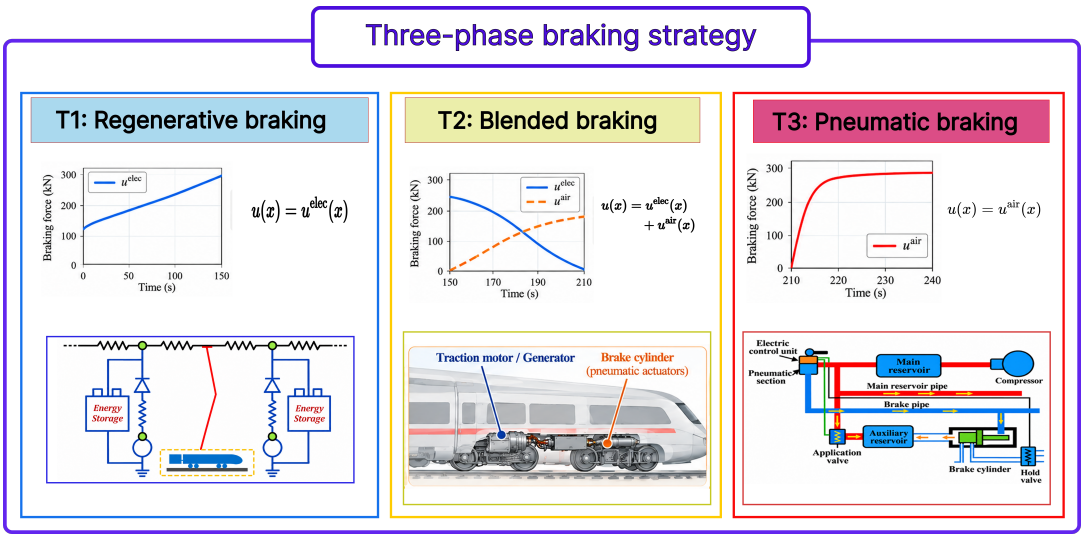


Figure 1. Conceptual illustration of the three-phase coordinated braking strategy for HSTs

The relationship between adhesion torque and adhesion force is expressed as

$$T_{a,i} = rF_{a,i}, \tag{9}$$

$$F_{a,i} = \mu_i(\lambda_i)Q_i, \tag{10}$$

and the slip ratio in braking mode is defined as

$$\lambda_i = \frac{v - r\omega_i}{\max(v, \varepsilon)} \tag{11}$$

where I_w is the moment of inertia of the wheelset; ω_i is the angular velocity of the ith wheelset; $T_{a,i}$ and $T_{b,i}$ are the adhesion torque and braking torque, respectively; m_v is the mass of the vehicle/carriage; $F_{a,i}$ is the adhesion force at the ith wheelset; F_{res} is the total resistance force; r is the wheel rolling radius; Q_i is the normal load; μ_i is the adhesion coefficient; λ_i is the slip ratio; and ε is a small positive constant introduced to avoid division by zero as v approaches zero. Figure 2 illustrates the force/torque balance of the vehicle and wheelset during braking.

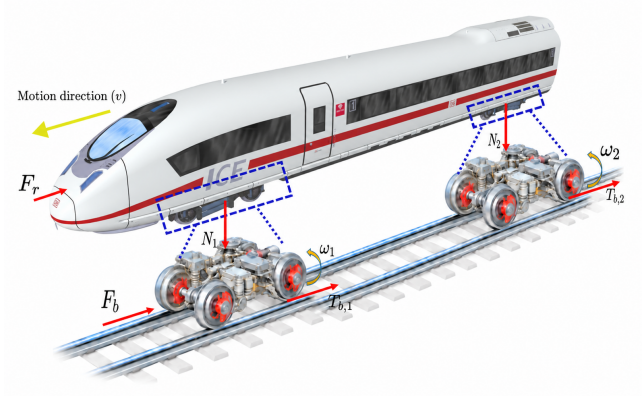


Figure 2. Longitudinal dynamic model of the train carbody, bogies, and wheelsets during braking [7]

Consistent with these force definitions, $F_{a,i}$ and μ_i in Eqs. (7)–(10) denote nonnegative braking-force and adhesion magnitudes; the corresponding longitudinal

force on the carriage is $-F_{a,i}$. In contrast, the LuGre force F_a in Eq. (14) is signed.

Wheel–rail adhesion is the nonlinear factor that determines the upper limit of braking force that can be transmitted through the wheel–rail contact. The relationship between the adhesion coefficient and slip ratio under different wheel–rail conditions is illustrated in Figure 3 [8]. To describe friction dynamics during active braking, Chen et al. employed the LuGre friction model for HSTs [8]. The relative slip velocity is defined as

$$v_s = r\omega - v, \tag{12}$$

the friction state satisfies

$$\dot{z} = v_s - \frac{\sigma_0 |v_s|}{g(v_s)} z, \tag{13}$$

and the adhesion force is expressed as

$$F_a = (\sigma_0 z + \sigma_1 \dot{z} + \sigma_2 v_s)\, F_z \tag{14}$$

The Stribeck function is given by

$$g(v_s) = \mu_c + (\mu_s - \mu_c) e^{-|v_s/v_s^*|^{1/2}} \tag{15}$$

where v_s is the relative slip velocity; z is the internal friction state; σ_0, σ_1, and σ_2 characterize the bristle stiffness, damping, and viscous friction, respectively; F_z is the normal load at the contact interface; μ_s and μ_c are the static friction coefficient and Coulomb friction coefficient, respectively; and v_s^* is the characteristic Stribeck velocity [8].

Recent wheel–rail studies have shown that adhesion varies significantly with creepage, speed, and surface-contact conditions. High-speed wheel–rail experiments under large-creepage and water conditions confirmed pronounced changes in adhesion with contact conditions [10]. The influence of adhesion on torsional vibration and braking-system stability was investigated in [41], while wheel–rail dynamic interaction under low-adhesion conditions and transient adhesion were studied in [42] and [43], respectively. For HSTs, wheel–rail adhesion has also been investigated from a multi-objective optimization perspective [44]. These results indicate that a fixed adhesion map cannot adequately represent the entire operating domain.

Remark 1. *The available braking-force range varies with adhesion, axle load, and actuator state. The usable braking force is limited by both wheel–rail adhesion, which depends on the adhesion coefficient and normal load, and the force available from the actuators; actuator delay also affects the braking-force response. Therefore, a braking controller based on a fixed nominal plant may have difficulty maintaining both stopping accuracy and wheel-slide safety over the entire operating range.*

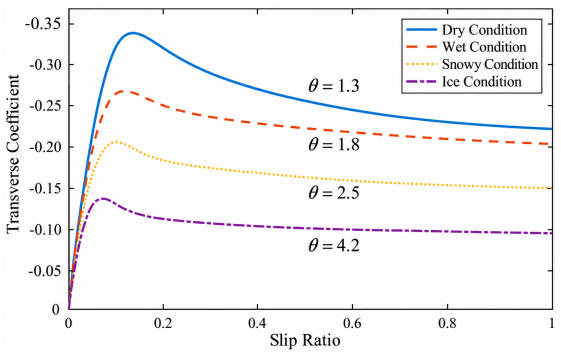


Figure 3. Relationship between adhesion coefficient and slip ratio under different wheel–rail conditions [8].

3. Artificial Intelligence for Braking Analysis and Control

AI studies related to braking can be categorized into three levels of representation and decision-making: feature-based ML, representation-based DL, and policy-based DRL. In this framework, ML transforms signals such as speed, position, axle speed, braking pressure, and contact features into structured features; DL directly learns nonlinear relationships from high-dimensional or time-series data; whereas DRL uses system states to generate actions through reward optimization. Therefore, these three groups differ not only in model depth but also in their roles within the control loop: estimation, prediction, and decision.

3.1. Machine Learning for Estimation and Braking-State Reconstruction

ML is suitable for problems where the input features have clear physical significance. The relationship between the feature vector x_k and the quantity to be estimated y_k can be expressed as

$$\hat{y}_k = f_\theta(\boldsymbol{x}_k), \tag{16}$$

where f_θ may represent an ANFIS model, random forest, gradient boosting, or an ensemble regressor. For supervised regression, the model parameters are trained by

$$\mathcal{L}_{\mathrm{ML}} = \frac{1}{N} \sum_{k=1}^{N} (y_k - \hat{y}_k)^2 \tag{17}$$

In train-control studies, Yang et al. employed ANFIS for speed tracking of high-speed electric multiple units and subsequently developed a multi-ANFIS approach to simultaneously model multiple motor/trailer cars [45], [35]. This multi-ANFIS structure is illustrated in Figure 4, where each car is represented by an ANFIS submodel and the outputs are combined to describe the state of the entire train [35]. Chen et al. used

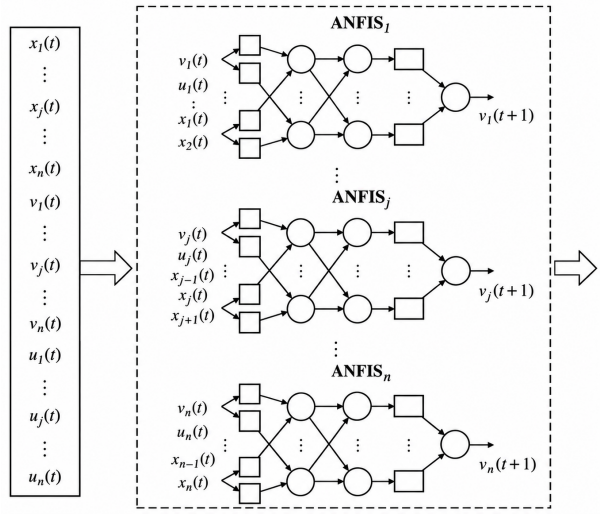


Figure 4. Multi-ANFIS structure used to model the dynamics of multiple cars in an HSEMU [35].

online learning to update the relationship between the approaching state and stopping error based on balise data [46], while soft-computing methods have also been applied to station parking [47]. More closely related to wheel–rail physics, Zirek and Uysal employed a voting-regression approach combining HistGBT, random forest, and linear regression to estimate the adhesion coefficient from measured data, achieving $R^2 = 0.922$ [27]. These results indicate that ML can replace or assist estimators that are difficult to construct analytically; however, estimation accuracy remains strongly dependent on the feature distribution and training domain.

3.2. Deep Learning for Nonlinear Features and Braking Time-Series Data

DL extends ML by learning representations directly from data rather than relying entirely on feature engineering. For a feed-forward network, the hidden state at layer l is defined as

$$\boldsymbol{h}^{(l)} = \sigma\left(W^{(l)}\boldsymbol{h}^{(l-1)} + \boldsymbol{b}^{(l)}\right), \tag{18}$$

while convolution extracts local patterns according to

$$h_j = \sigma\left(b_j + \sum_{i=0}^{K-1} w_i x_{j-i}\right). \tag{19}$$

For time-dependent braking signals, LSTM maintains the cell state through a gating mechanism.

$$\begin{aligned} f_k &= \sigma(W_f[x_k, h_{k-1}] + b_f), \\ i_k &= \sigma(W_i[x_k, h_{k-1}] + b_i), \\ C_k &= f_k \odot C_{k-1} + i_k \odot \tilde{C}_k, \quad h_k = o_k \odot \tanh C_k \end{aligned} \tag{20}$$

Chen et al. developed DNN, CNN, and few-shot CNN models using real operational data from the Beijing–Shenyang high-speed railway. The DNN learns the mapping between position–velocity histories and braking distance; the CNN captures local relationships, while the few-shot CNN addresses the scarcity of samples with large parking errors. Compared with the method currently used in practice, the stopping error was reduced by 38.6%, 42.8%, and 49.2%, respectively [25]. At the wheel level, Namoano et al. combined wavelet analysis, LSTM, and neural-network classification to detect wheel slip from axle-speed and brake-pressure signals collected from trains in actual operation [26]. This approach demonstrates that DL can capture temporal structures and high-dimensional correlations more effectively than conventional feature-based models; however, its outputs remain primarily prediction or classification results rather than safety-guaranteed braking actions.

3.3. Deep Reinforcement Learning for Braking Decision-Making

DRL shifts the problem from estimation to sequential decision-making. The environment is modeled as a Markov decision process

$$\mathcal{M} = (\mathcal{S}, \mathcal{A}, P, R, \gamma), \tag{21}$$

where the state may include position, speed, wheel speed, slip, adhesion estimate, and actuator state; the action is the traction/braking command. The cumulative return is defined as

$$G_k = \sum_{j=0}^{\infty} \gamma^j r_{k+j}, \tag{22}$$

and the optimal action-value function satisfies the Bellman relation

$$Q^*(s,a) = \mathbb{E}\left[r + \gamma \max_{a'} Q^*(s', a')\right] \tag{23}$$

The objective of the policy is

$$J(\pi) = \mathbb{E}_\pi[G_k] \tag{24}$$

Lu and Liu combined dueling networks, double DQN, and prioritized replay, reducing energy consumption by 15.75% and increasing convergence speed by about 37% against the operational baseline [36]. Shang et al. used a reference system to correct constraint violations during learning, improving convergence and energy efficiency [48]. Huang et al. combined expert knowledge with PPO for safety, punctuality, energy, and comfort, enabling online metro traction/braking decisions without a fixed offline speed profile [49].

Remark 2. *AI enhances estimation, representation, and decision-making capabilities; however, the physical feasibility of braking actions still depends on adhesion and actuator states. The remaining gap is to integrate online physical updating with policy learning and a mechanism that guarantees action feasibility before commands are transmitted to the braking system.*

4. CTD4–Digital Twin Framework for Active Braking

The review above indicates that a next-generation braking controller should integrate two layers of information. Figure 5 illustrates the proposed CTD4–Digital Twin framework for active HST braking. The first layer is physical braking dynamics, in which actuator delay, wheel slip, wheel–rail adhesion, and EB–AB limits determine the feasible action domain. The second layer is the learning layer, where the policy must adapt to disturbances, parameter variations, and changing operating conditions without relying entirely on a nominal plant. Based on the two identified information layers, Digital Twin is used to link the physical characteristics of the braking system with the control decision-making process [50]. Through this connection, train dynamics models, regenerative braking, pneumatic braking, and wheel and rail adhesion are integrated into Digital Twin to represent the physical characteristics of the high-speed train braking system. The updated states and parameters from these models provide information to the augmenting layer, supporting the brake control decision-making process as adhesion conditions and actuator characteristics change.

To connect the physical and learning layers, the DT in the proposed architecture receives train speed, wheel angular speed, braking pressure, EB/AB states, and related signals to maintain the synchronized state $\hat{\mathbf{x}}_k^{DT}$ and the parameter vector $\hat{\boldsymbol{\theta}}_k$. The updated twin state is then used to construct the input to CTD4 rather than relying only on raw plant measurements. Accordingly, CTD4 receives a twin-augmented state comprising measured states, estimated adhesion, actuator condition, and model-prediction error. This allows the learning policy to respond to variations in the braking plant while retaining estimators and constraints derived from the physical braking model. Current railway DT studies mainly focus on monitoring, health estimation, model validation, and decision support [32], [34], [37]. However, their direct integration with learning-based braking control remains limited.

The main contribution of the proposed framework is the integration of CTD4 with Digital Twin state and parameter updating and railway-specific safety projection. While the distributional learning mechanism follows the original CTD4 method [38], the proposed integration incorporates wheel–rail adhesion, actuator conditions, and physical braking constraints into the control architecture.

CTD4 extends the deterministic actor–critic architecture of TD3 to a continuous distributional formulation, in which each critic outputs the mean and standard deviation of a Gaussian return distribution [38]. For critic i, the return distribution is represented as

$$Z_{\theta_i}(s,a) = \mathcal{N}\big(\mu_i(s,a), \sigma_i^2(s,a)\big), \quad i = 1, \ldots, N. \tag{25}$$

The Gaussian notation $\mathcal{N}(\mu, \sigma^2)$ in Eqs. (25)–(27) denotes a distribution with mean μ and variance σ^2; σ denotes standard deviation.

Following CTD4 [38], two critic distributions are combined by the Kalman-inspired rule

$$\begin{aligned} K_i &= \frac{\sigma_i^2}{\sigma_i^2 + \sigma_{i+1}^2}, \qquad \mu_F = \mu_i + K_i(\mu_{i+1} - \mu_i), \\ \sigma_F^2 &= (1 - K_i)\sigma_i^2 + K_i\sigma_{i+1}^2. \end{aligned} \tag{26}$$

This fusion rule follows Eqs. (1)–(3) of CTD4 [38]. Its variance differs from the standard independent-Gaussian posterior, $\sigma_F^2 = (1 - K_i)\sigma_i^2$. It is retained as a heuristic aggregation rule, without claiming minimum-variance optimality or guaranteed uncertainty reduction.

The fused parameters (μ_F, σ_F) define the Gaussian return distribution used to construct the distributional Bellman target,

$$Z_{\text{target}} = R + \gamma Z(\mu_F, \sigma_F) = \mathcal{N}\big(R + \gamma\mu_F,\ (\gamma\sigma_F)^2\big). \tag{27}$$

The deterministic actor is updated using the mean of the fused return distribution. For a mini-batch of M transitions, the policy gradient is

$$\nabla_\phi J(\phi) \approx \frac{1}{M}\sum_{j=1}^{M} \nabla_a \mu_F(s_j, a)\Big|_{a=\pi_\phi(s_j)} \nabla_\phi \pi_\phi(s_j). \tag{28}$$

The DT updates its state and parameters based on a prediction-correction approach.

$$\begin{aligned} \hat{x}_{k+1}^{DT} &= f_{DT}\left(\hat{x}_k^{DT}, u_k, \hat{\theta}_k\right), \\ \hat{\theta}_{k+1} &= \hat{\theta}_k + L_k\left[y_k - h\left(\hat{x}_k^{DT}, \hat{\theta}_k\right)\right]. \end{aligned} \tag{29}$$

The update gain L_k determines how the measurement–prediction residual contributes to parameter correction. The estimated parameter vector includes wheel–rail adhesion characteristics and actuator parameters, such as adhesion-model coefficients and response time constants. These updated estimates provide physical information for CTD4-based braking decisions and the safety projection in Eq. (30).

Finally, the action generated by CTD4 is not transmitted directly to the braking actuator but is projected onto the feasible action set.

$$u_k^* = \arg\min_{u \in \mathcal{U}_{\text{safe}}(\hat{x}_k^{DT}, \hat{\theta}_k)} \|u - u_{\text{CTD4},k}\|_2^2. \tag{30}$$

where $u_{\text{CTD4},k} = \pi_\phi(s_k^{DT})$ denotes the unconstrained action generated by CTD4, while $\mathcal{U}_{\text{safe}}$ defines the

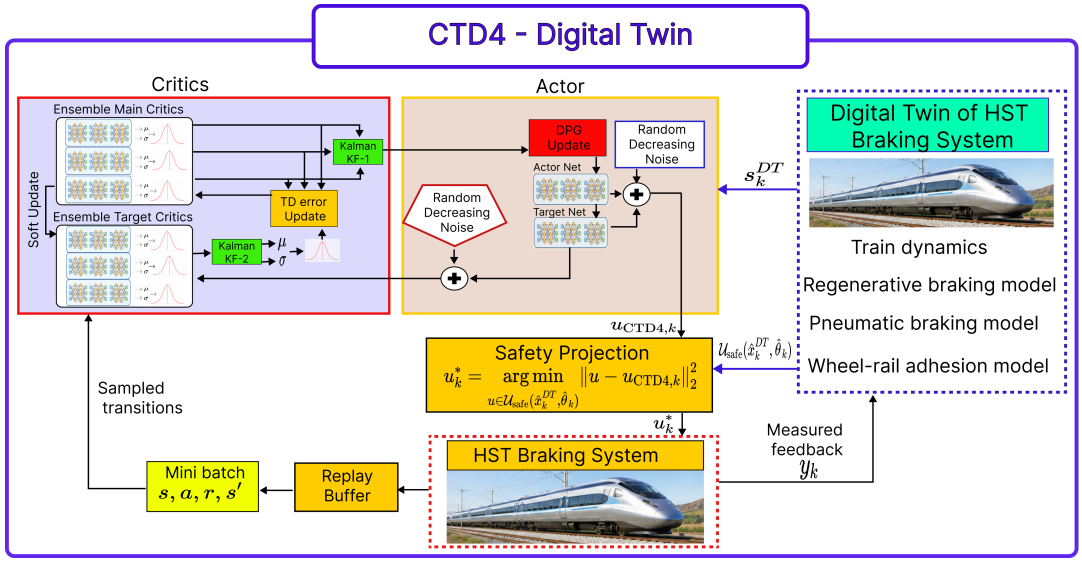


Figure 5. Proposed CTD4–Digital Twin framework for active HST braking.

physically feasible action set according to EB/AB capability, pressure and torque saturation, slip bounds, and jerk limits. In this framework, the DT accounts for the plant variations identified in Remark 1, whereas CTD4 combined with the safety projection addresses the gap between adaptability and hard physical constraints highlighted in Remark 2. This coupling forms the core logic of the proposed CTD4–DT framework.

The proposed framework integrates DT updating, CTD4 policy inference, and safety projection into a coordinated braking-control process. The DT updates wheel–rail adhesion and actuator parameters to support braking decisions under varying operating conditions. The computational requirements of these components are considered in relation to the braking control cycle to assess real-time implementation feasibility.

The framework still needs to be tested. Simulation cases should include changes between dry, wet, and low-adhesion conditions, together with actuator delays, parameter errors, and sensor noise. Multi-domain simulation [51] and embedded-control studies [52] offer useful references for implementation. HIL tests would then precede brake or wheelset experiments, following the testing approaches in [53], [54]. These experiments would examine pressure response, peak slip, and whether the requested torque can be delivered. Evaluation also needs to account for adhesion and regenerative-braking utilization. The monitoring, estimation, and decision-support functions studied in railway DT applications [32], [37] provide a basis for developing this connection between the twin, controller, and safety projection.

5. Conclusion

The proposed CTD4–DT framework provides a structured approach to integrating physical-state estimation, learning-based braking control, and safety constraints. The DT updates adhesion and actuator information, while the safety projection adjusts braking commands according to the estimated operating limits. The framework also identifies the main requirements for practical implementation, including computational feasibility, estimation accuracy, and braking performance under varying adhesion conditions. These aspects provide a basis for further evaluation through simulation, HIL testing, and brake or wheelset experiments.

Acknowledgements

The authors acknowledge the academic support of the AIT Research Group, University of Transport Ho Chi Minh City.

References

[1] A. Anagnostopoulos, “High-speed railway and safety: Insights from a bibliometric approach,” *High-Speed Railway*, vol. 2, no. 3, pp. 187–196, 2024, doi: 10.1016/j.hspr.2024.08.004.

[2] C.-F. Lu, “A discussion on technologies for improving the operational speed of high-speed railway networks,” *Transp. Saf. Environ.*, vol. 1, no. 1, pp. 22–36, 2019, doi: 10.1093/tse/tdz003.

[3] J. Wang, Z. Chen, Z. Chen, C. Yang, and W. Gui, “A survey of braking control techniques for railway vehicles,” *Sci. China Inf. Sci.*, vol. 69, Art. no. 131201, 2026, doi: 10.1007/s11432-025-4671-y.

[4] R. Pfaff, *Railway Brake Systems: Framework, Requirements, and Solutions*. Cham, Switzerland: Springer, 2025, doi: 10.1007/978-3-031-69958-0.

[5] F. Guo and J. He, "Optimal allocation method of electric/air braking force of high-speed train considering axle load transfer," *High-Speed Railway*, vol. 2, no. 2, pp. 77–84, 2024, doi: 10.1016/j.hspr.2024.04.004.

[6] J. Wang, Z. Chen, Z. Chen, and W. Gui, "A decentralised braking force distribution strategy for high-speed trains," *IET Intell. Transp. Syst.*, 2025, doi: 10.1049/itr2.70100.

[7] S. Shrestha, M. Spiryagin, and Q. Wu, "Friction condition characterization for rail vehicle advanced braking system," *Mech. Syst. Signal Process.*, vol. 134, Art. no. 106324, 2019, doi: 10.1016/j.ymssp.2019.106324.

[8] B. Chen, Z. Huang, R. Zhang, F. Jiang, W. Liu, H. Li, J. Wang, and J. Peng, "Adaptive slip ratio estimation for active braking control of high-speed trains," *ISA Trans.*, vol. 112, pp. 302–314, 2021, doi: 10.1016/j.isatra.2020.11.027.

[9] Y. Jin, G. Xie, P. Chen, X. Hei, W. Ji, and J. Zhao, "High-speed train emergency brake modeling and online identification of time-varying parameters," *Math. Probl. Eng.*, vol. 2020, Art. no. 3872852, pp. 1–13, 2020, doi: 10.1155/2020/3872852.

[10] C. Chang, B. Chen, Y. Cai, and J. Wang, "Experimental investigation of high-speed wheel-rail adhesion characteristics under large creepage and water conditions," *Wear*, vols. 540–541, Art. no. 205254, 2024, doi: 10.1016/j.wear.2024.205254.

[11] T. D. Tran, C. S. Doan, T. D. Le, V. D. Do, and X. K. Dang, "Suspension control strategies for high-speed trains: A comprehensive review and future perspectives," *J. Current Sci. Technol.*, vol. 16, no. 3, Art. no. 206, 2026, doi: 10.59796/jcst.V16N3.2026.206.

[12] P. Havaei and M. A. Sandidzadeh, "Intelligent-PID controller design for speed track in automatic train operation system with heuristic algorithms," *J. Rail Transp. Plan. Manag.*, vol. 22, Art. no. 100321, 2022, doi: 10.1016/j.jrtpm.2022.100321.

[13] X. Wang and T. Tang, "Optimal operation of high-speed train based on fuzzy model predictive control," *Adv. Mech. Eng.*, vol. 9, no. 3, pp. 1–14, 2017, doi: 10.1177/1687814017693192.

[14] Y. Guo, P. Sun, X. Feng, and K. Yan, "Adaptive fuzzy sliding mode control for high-speed train using multi-body dynamics model," *IET Intell. Transp. Syst.*, vol. 17, pp. 450–461, 2023, doi: 10.1049/itr2.12270.

[15] Z. Li, D. Huang, and L. Cai, "Adaptive nonsingular terminal sliding mode tracking control for high-speed trains with input constraints and parametric uncertainties," *Int. J. Control Autom. Syst.*, vol. 22, pp. 753–764, 2024, doi: 10.1007/s12555-022-0659-6.

[16] Z. Li, L. Zhou, H. Yang, and Y. Yan, "Model-free adaptive robust control method for high-speed trains," *Transp. Saf. Environ.*, vol. 6, no. 1, Art. no. tdad013, 2024, doi: 10.1093/tse/tdad013.

[17] L. Zhou, Z. Li, H. Yang, and C. Tan, "Integral predictive sliding mode control for high-speed trains: A dynamic linearization and input constraint-based data-driven scheme," *Control Eng. Pract.*, vol. 154, Art. no. 106139, 2025, doi: 10.1016/j.conengprac.2024.106139.

[18] J. Wang, Z. Chen, and Z. Chen, "Model predictive control for high-speed train braking systems with priority-based force distribution," *IEEE Trans. Control Syst. Technol.*, vol. 34, no. 4, pp. 2162–2169, 2026, doi: 10.1109/TCST.2026.3685687.

[19] V.-D. Do, X.-K. Dang, S. Ly, and N.-T. Nguyen, "Positioning the semi-submersible platform using model predictive control with thruster constraints," in *Proc. 2023 Asia Meeting on Environment and Electrical Engineering (EEE-AM)*, 2023, doi: 10.1109/EEE-AM58328.2023.10395200.

[20] X.-P. Nguyen, X.-K. Dang, V.-D. Do, J. M. Corchado, and H.-N. Truong, "Robust Adaptive Fuzzy-Free Fault-Tolerant Path Planning Control for a Semi-Submersible Platform Dynamic Positioning System With Actuator Constraints," *IEEE Trans. Intell. Transp. Syst.*, vol. 24, no. 11, pp. 12701–12715, 2023, doi: 10.1109/TITS.2023.3297252.

[21] X.-K. Dang, V.-D. Do, and Z. Koboevic, "Short-term Motion Control for Semi-submersible Platform Based on Constrained Fuzzy Genetic Optimization Controller," *Adv. Electr. Comput. Eng.*, vol. 25, no. 3, pp. 79–92, 2025, doi: 10.4316/AECE.2025.03009.

[22] X.-K. Dang, V.-D. Do, N.-T. Nguyen, and S. Ly, "Integrating model predictive control with deep learning for sway reduction in ship-to-shore crane operations," *EAI Endorsed Trans. Transp. Syst. Ocean Eng.*, vol. 1, no. 1, 2025, doi: 10.4108/tsoe.10838.

[23] T.-D. Nguyen, T.-D. Nguyen, T.-T. Pham, and V.-M. Nguyen, "Speed control of marine diesel engine based on Lyapunov neural network combined with adaptive backpropagation algorithm," *EAI Endorsed Trans. Transp. Syst. Ocean Eng.*, vol. 1, no. 1, 2025, doi: 10.4108/tsoe.11168.

[24] X.-K. Dang, J. M. Corchado, V.-V. Le, and V.-D. Do, "Non-parametric vibration-based structural damage detection for coastal structures: Multi-dimension to single input convolutional neural network approach," *Adv. Electr. Comput. Eng.*, vol. 24, no. 4, pp. 3–18, 2024, doi: 10.4316/AECE.2024.04001.

[25] X. Chen, J. Yin, and C. Ning, "Intelligent train stopping control for railways: A deep learning approach," *IET Intell. Transp. Syst.*, vol. 17, no. 10, pp. 1935–1950, 2023, doi: 10.1049/itr2.12385.

[26] B. Namoano, C. Emmanouilidis, and A. Starr, "Detecting wheel slip from railway operational data through a combined wavelet, long short-term memory and neural network classification method," *Eng. Appl. Artif. Intell.*, vol. 137, Part B, Art. no. 109173, 2024, doi: 10.1016/j.engappai.2024.109173.

[27] A. Zirek and C. Uysal, "A machine learning based voting regression method for adhesion estimation in wheel-rail contact," *Veh. Syst. Dyn.*, vol. 63, no. 10, pp. 1920–1937, 2025, doi: 10.1080/00423114.2024.2390578.

[28] H. Ni, Q. Fu, J. Easton, N. Zhao, and T. N. Arvanitis, "Reinforcement learning in railway research and applications: A review," *Transp. Res. Interdiscip. Perspect.*, vol. 39, Art. no. 102165, 2026, doi: 10.1016/j.trip.2026.102165.

[29] L. Ning, M. Zhou, Z. Hou, R. M. P. Goverde, F.-Y. Wang, and H. Dong, "Deep deterministic policy gradient for high-speed train trajectory optimization," *IEEE Trans. Intell. Transp. Syst.*, vol. 23, no. 8, pp.

11562–11574, 2022, doi: 10.1109/TITS.2021.3105380.

[30] M. Zhou, X. Liu, H. Wang, and H. Dong, "Memory-based TD3 for autonomous train speed trajectory optimization under virtual coupling," *IEEE Trans. Intell. Transp. Syst.*, vol. 27, no. 4, pp. 3973–3985, 2026, doi: 10.1109/TITS.2026.3667481.

[31] J. Lin, X. Qiu, and M. Li, "Tracking interval control for urban rail trains based on safe reinforcement learning," *Eng. Appl. Artif. Intell.*, vol. 137, Art. no. 109226, 2024, doi: 10.1016/j.engappai.2024.109226.

[32] E. A. Thompson, P. Lu, P. K. Alimo, H. B. Atuobi, E. T. Akoto, and C. K. Abbew, "Revolutionizing railway systems: A systematic review of digital twin technologies," *High-Speed Railway*, vol. 3, no. 3, pp. 238–250, 2025, doi: 10.1016/j.hspr.2025.05.005.

[33] Z. Y. Zhang, D. Shang, and S. Su, "Digital twin in railway industry: A bibliometric analysis and systematic review," *Digital Twin*, vol. 3, no. 1, Art. no. 2533858, 2026, doi: 10.1080/27525783.2025.2533858.

[34] D. Ershenko, G. Derbysheva, A. Panayi, and C. Fortin, "Quantitative metrics for validation and decision-making in digital twins: A comparative study on a railway braking system," *Proc. Des. Soc.*, vol. 5, pp. 2671–2680, 2025, doi: 10.1017/pds.2025.10281.

[35] H. Yang, Y. Fu, and D. Wang, "Multi-ANFIS model based synchronous tracking control of high-speed electric multiple unit," *IEEE Trans. Fuzzy Syst.*, vol. 26, no. 3, pp. 1472–1484, 2018, doi: 10.1109/TFUZZ.2017.2725819.

[36] T. Lu and B. Liu, "Automatic driving operation strategy of urban rail train based on improved DQN algorithm," *J. Artif. Intell.*, vol. 5, pp. 113–129, 2023, doi: 10.32604/jai.2023.043970.

[37] J. Peng et al., "A Digital Twin-Driven Hybrid Estimate Method for Health Status of Train Braking System," in *Proc. 2022 IEEE 25th Int. Conf. Comput. Supported Cooperative Work in Design (CSCWD)*, pp. 335–340, 2022, doi: 10.1109/CSCWD54268.2022.9776057.

[38] D. Valencia, H. Williams, Y. Xing, T. Gee, B. A. MacDonald, and M. Liarokapis, "CTD4 – a Deep Continuous Distributional Actor-Critic Agent with a Kalman Fusion of Multiple Critics," Proc. AAAI Conf. Artif. Intell., vol. 39, no. 20, pp. 20956–20963, 2025, doi: 10.1609/aaai.v39i20.35391.

[39] A. Cunillera, N. Besinovic, R. M. Lentink, N. van Oort, and R. M. P. Goverde, "A literature review on train motion model calibration," IEEE Trans. Intell. Transp. Syst., vol. 24, no. 4, pp. 3660–3677, 2023, doi: 10.1109/TITS.2023.3236062.

[40] Q. Wu et al., "Freight train air brake models," Int. J. Rail Transp., vol. 11, no. 1, pp. 1–49, 2023, doi: 10.1080/23248378.2021.2006808.

[41] Q. Wang, Z. Wang, J. Mo, R. Wang, and K. Wang, "Effect and mechanism of wheel-rail adhesion on torsional vibration and stability of the braking system," *Tribol. Int.*, vol. 179, Art. no. 108182, 2023, doi: 10.1016/j.triboint.2022.108182.

[42] C. Lu, D. Chen, J. Shi, and Z. Li, "Research on wheel-rail dynamic interaction of high-speed railway under low adhesion condition," *Eng. Fail. Anal.*, vol. 157, Art. no. 107935, 2024, doi: 10.1016/j.engfailanal.2023.107935.

[43] D. Kvarda, A. Meierhofer, and K. Six, "Testing and modelling of transient adhesion phenomena in rolling-sliding contacts," *Friction*, vol. 12, pp. 1016–1027, 2024, doi: 10.1007/s40544-023-0825-8.

[44] C. Huang, X. Zhou, Y. Chen, L. Jing, and K. Wang, "Multi-objective optimisation of wheel-rail adhesion for high-speed trains with aerodynamic lift wings," *Veh. Syst. Dyn.*, vol. 63, no. 2, pp. 375–397, 2025, doi: 10.1080/00423114.2024.2342533.

[45] H. Yang, Y.-T. Fu, K.-P. Zhang, and Z.-Q. Li, "Speed tracking control using an ANFIS model for high-speed electric multiple unit," *Control Eng. Pract.*, vol. 23, pp. 57–65, 2014, doi: 10.1016/j.conengprac.2013.10.006.

[46] D. Chen, R. Chen, Y. Li, and T. Tang, "Online learning algorithms for train automatic stop control using precise location data of balises," *IEEE Trans. Intell. Transp. Syst.*, vol. 14, no. 3, pp. 1526–1535, 2013, doi: 10.1109/TITS.2013.2265171.

[47] D. Chen and C. Gao, "Soft computing methods applied to train station parking in urban rail transit," *Appl. Soft Comput.*, vol. 12, pp. 759–767, 2012, doi: 10.1016/j.asoc.2011.10.016.

[48] M. Shang, Y. Zhou, and H. Fujita, "Deep reinforcement learning with reference system to handle constraints for energy-efficient train control," *Inf. Sci.*, vol. 570, pp. 708–721, 2021, doi: 10.1016/j.ins.2021.04.088.

[49] Y. Huang, W. Lai, D. Chen, G. Lin, and J. Yin, "Enhanced intelligent train operation algorithms for metro train based on expert system and deep reinforcement learning," *PLOS ONE*, vol. 20, no. 5, Art. no. e0323478, 2025, doi: 10.1371/journal.pone.0323478.

[50] Q. Wu, M. Spiryagin, P. Liu, C. Cole, and E. Bernal, "Co-simulation methods for train braking dynamics," *Proc. Inst. Mech. Eng., Part F: J. Rail Rapid Transit*, vol. 237, no. 8, pp. 1072–1081, 2023, doi: 10.1177/09544097231155564.

[51] H. P. Nguyen, V. D. Doan, T. S. Nguyen, V. H. Cao, and V. C. Pham, "Simulation and Analysis of Vehicle Dynamics Using Simcentre Amesim," *EAI Endorsed Transactions on Transportation Systems and Ocean Engineering*, vol. 2, no. 1, 2026, doi: 10.4108/tsoe.11473.

[52] X.-K. Dang, V.-D. Do, T.-D. Tran, and S. Ly, "Real-Time Embedded Control for the Propulsion System of Semi-submersible Platform," in *Proc. 10th International Conference on Coastal and Ocean Engineering*, pp. 350–362, 2024, doi: 10.1007/978-981-97-5353-6_27.

[53] L. Pugi, G. Paolieri, M. Giorgetti, L. Berzi, R. Viviani, L. Cabrucci, and L. Bocciolini, "HIL testing of wheel slide protection systems: Criteria for continuous updating and validation," Railway Eng. Sci., vol. 31, pp. 108–121, 2023, doi: 10.1007/s40534-022-00298-7.

[54] J. Zhou and M. Wu, "Design of hardware-in-the-loop test bench for braking and anti-skid of trains," in *Urban Transport XXVI*, WIT Trans. Built Environ., vol. 200, pp. 155–167, 2020, doi: 10.2495/UT200131.